

# Voltage-Driven Molecular Catalysis of Electrochemical Reactions

Koushik Barman,<sup>†,‡</sup> Xiang Wang,<sup>†,§,‡</sup> Rui Jia,<sup>†,§</sup> Gaukhar Askarova,<sup>†,§</sup> Guoxiang Hu,<sup>†,§,\*</sup> and Michael V. Mirkin<sup>†,‡,\*</sup>

<sup>†</sup> Department of Chemistry and Biochemistry, Queens College-CUNY, Flushing, NY 11367, USA.

<sup>§</sup> The Graduate Center of CUNY, New York, NY 10016.

<sup>#</sup> Advanced Science Research Center at The Graduate Center, CUNY; New York, NY 10031.

*Supporting Information Placeholder*

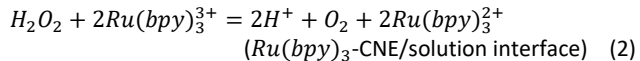
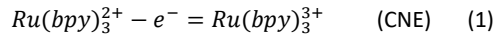
**ABSTRACT:** Heterogeneous electrocatalysis and molecular redox catalysis have developed over several decades as two distinct ways to facilitate charge-transfer processes essential for energy conversion and storage. Whereas electrocatalytic reactions are driven by the applied voltage, molecular catalytic processes are driven by the difference between standard potentials of the catalyst and the reactant. Here we demonstrate that the rate of electron transfer between a dissolved reactant and a molecular catalyst immobilized directly on the surface of a carbon nanoelectrode is governed by combination of chemical driving force and electrostatic potential drop across the double layer. DFT calculations show that varying the applied voltage alters the potential drop between the surface-bound and dissolved redox species. These results suggest a new route for designing next-generation hybrid molecular/electrocatalysts.

The integration of the concepts of electrocatalysis and molecular catalysis of redox reactions has recently become a popular approach to developing sufficiently active and durable catalysts for water oxidation, hydrogen evolution, and other processes central to energy conversion and storage.<sup>1-3</sup> A conventional molecular catalyst is a reversible redox couple either dispersed in electrolyte solution or immobilized on the electrode surface in a monolayer or multi-layer film.<sup>4</sup> The charge transfer occurs between the active form of the catalyst and the dissolved substrate species, and the electrode material does not chemically participate in the catalytic reaction.<sup>5</sup> By contrast, an electrocatalytic reaction occurs on active surface sites, and the chemical nature of the electrode material as well as its surface features and defect density largely determine the catalytic efficiency.<sup>6,7</sup> Recent studies focused on similarity of concepts in these fields and highlighted the advantages of combining these catalyst types into hybrid systems.<sup>1-3,8-12</sup> For instance, it was suggested that the applied bias affects the activation free energy and rate of electrocatalytic oxygen evolution reaction (OER) on iridium oxide through charge accumulation in the catalyst.<sup>8</sup> Conversely, electronically coupling a molecular catalyst to an electrode can yield higher rates at low overpotentials by eliminating redox intermediates.<sup>13</sup> Field-driven catalysis of oxidation and reduction reactions occurring simultaneously at a conductive particle floating at the liquid/liquid interface has also been reported.<sup>14</sup>

The electrode bias plays different roles in conventional molecular catalysis and electrocatalysis. In the former, the applied voltage only drives the outer-sphere oxidation or reduction of the

redox catalyst, whereas in the latter it drives the direct inner-sphere electron transfer (ET) between the electrode and substrate molecules.<sup>5,15</sup> Here we show that potential drop can contribute to the driving force for ET between a molecular catalyst immobilized directly on the electrode surface and a dissolved reactant. In this way a bimolecular ET reaction can be driven uphill, and a molecular catalyst can oxidize (or reduce) various substrates with more positive (or negative) standard potentials, e.g., ferrocenium ( $\text{Fc}^+$ ) or trisbipyridineruthenium ( $\text{Ru}(\text{bpy})_3^{3+}$ ) can oxidize hydrogen peroxide and water.

Recently reported mediated charge-transfer reactions between redox moieties attached directly (i.e., without a spacer) to the surface of a carbon nanoelectrode (CNE)<sup>16</sup> and various substrates dissolved in an aqueous solution include the oxidation of hydrogen peroxide by surface-bound  $\text{Ru}(\text{bpy})_3^{3+}$ :



A steady-state voltammogram of this process (curve 1 in Figure 1A recorded point-by-point; see Figure S1 and Supporting Information for experimental details) exhibits the onset of current at the potential,  $E \approx +0.8$  V vs. Ag/AgCl reference that corresponds to the beginning of  $\text{Ru}(\text{bpy})_3^{2+}$  oxidation<sup>16</sup> (Reaction 1; Figure S2). At  $E = 1.0$  V, essentially all surface-bound  $\text{Ru}(\text{bpy})_3^{2+}$  species are converted to  $\text{Ru}(\text{bpy})_3^{3+}$ , and the current–potential ( $i$ – $E$ ) dependence in Figure 1A levels off to the value of  $\sim 180$  pA corresponding to the kinetic current of Reaction 2.<sup>16</sup> This value is  $\sim 1/3$  of the diffusion-limited current of 10 mM  $\text{H}_2\text{O}_2$  to the surface of the 50-nm-radius CNE ( $i_{\text{diff}} \approx 630$  pA; Supporting Information). At a more positive CNE bias,  $i$  increases over a wide potential range ( $\sim 400$  mV) and eventually reaches the diffusion-limited value. This increase cannot be attributed to direct oxidation of  $\text{H}_2\text{O}_2$  on the bare carbon surface because the current produced by this process (curve 2 in Figure 1A) is orders of magnitude lower than that in curve 1. The current measured at the same  $\text{Ru}(\text{bpy})_3$ -modified CNE ( $\text{Ru}(\text{bpy})_3\text{-CNE}$ ) with no  $\text{H}_2\text{O}_2$  is also very low at  $E \leq 1.45$  V vs. Ag/AgCl (curve 1 in Figure 1B). We hypothesize that the rate of Reaction 2 increases with applied potential due to the contribution of the voltage drop between the  $\text{Ru}(\text{bpy})_3^{3+}$  moieties on the carbon surface and the dissolved  $\text{H}_2\text{O}_2$  molecules that can approach the electrode only as close as the outer Helmholtz plane (OHP).<sup>17</sup>

Another example of voltage-driven molecular redox catalysis is OER at the  $\text{Ru}(\text{bpy})_3\text{-CNE}$  (curve 1 in Figure 1B). Since the standard

potential of the  $\text{Ru}(\text{bpy})_3^{3/2+}$  couple ( $E^\circ = 1.24$  V vs NHE)<sup>18</sup> is not high enough to provide a sufficient driving force for fast water oxidation, the current in Figure 1B remains immeasurably low after the complete oxidation of  $\text{Ru}(\text{bpy})_3^{2+}$  to  $\text{Ru}(\text{bpy})_3^{3+}$ , i.e., at  $1 \text{ V} < E \leq 1.4$  V vs. Ag/AgCl. At a higher anodic bias, the OER current increases markedly over  $\sim 600$  mV potential range. By contrast, the water oxidation at a similarly sized bare CNE is very slow (curve 2 in Figure 1B), suggesting that the current in curve 1 is produced by ET between water molecules and  $\text{Ru}(\text{bpy})_3^{3+}$  driven by the applied potential.

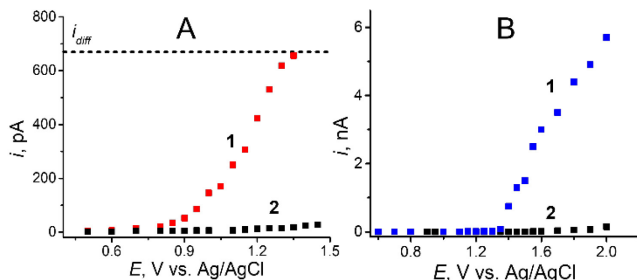


**Figure 1.** Steady-state voltammograms of  $\text{H}_2\text{O}_2$  (A) and water (B) oxidation at  $\text{Ru}(\text{bpy})_3$ -CNE (curves 1) and bare CNE (curves 2). The electrode radius,  $a \approx 50$  nm. Electrolyte solution was: (A) 10 mM  $\text{H}_2\text{O}_2$  in 0.1 M PBS; and (B) 0.1 M PBS.

Field-driven bimolecular ET processes have also been observed with different surface-bound redox mediators. The voltammogram of a ferrocene modified CNE (Fc-CNE) in 40 mM  $\text{H}_2\text{O}_2$  solution (curve 1 in Figure 2A) shows high anodic current, whereas the current measured at the same nanoelectrode without  $\text{H}_2\text{O}_2$  (curve 1 in Figure S3) is incomparably lower. No oxidation wave of  $\text{H}_2\text{O}_2$  was observed at a bare CNE under the same conditions (curve 2 in Figure 1A). The onset of the  $\text{H}_2\text{O}_2$  oxidation current in Figure 2A (the inset) is  $\sim 300$  mV less positive than that in Figure 1A due to a much lower standard potential of the  $\text{Fc}^+/\text{Fc}$  couple ( $E^\circ = 0.4$  V vs NHE).<sup>19</sup> The measurable anodic current in Figure 2A appears at  $\sim 0.5$  V vs. Ag/AgCl, which is about 250 mV higher than the potential corresponding to the complete oxidation of Fc moieties. The subsequent rise in the  $i - E$  curve over  $\sim 700$  mV potential range represents voltage-assisted oxidation of  $\text{H}_2\text{O}_2$  by  $\text{Fc}^+$ . This process is driven by the applied electrode potential because the  $E^\circ$  of the  $\text{Fc}^+/\text{Fc}$  couple is more negative than  $E^\circ$  of  $\text{H}_2\text{O}_2$  (0.7 V vs NHE),<sup>18</sup> and the chemical driving force for oxidation of  $\text{H}_2\text{O}_2$  by  $\text{Fc}^+$  is too small to produce measurable current at  $E < \sim 0.5$  V vs. Ag/AgCl. Figure S5 shows no homogeneous catalysis of  $\text{H}_2\text{O}_2$  oxidation by

dissolved Fc. The current of direct  $\text{H}_2\text{O}_2$  oxidation at a bare CNE (curve 2 in Figure 2A) is negligible in comparison with the Fc mediated ET current.

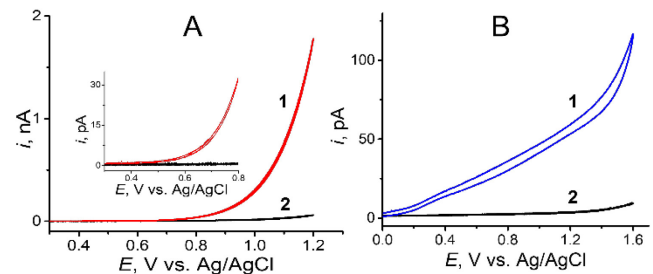


**Figure 2.** Steady-state voltammograms of  $\text{H}_2\text{O}_2$  (A) and hydrazine (B) oxidation at Fc-CNE (curves 1) and bare CNE (curves 2). The CNE radius,  $a \approx 50$  nm. Solution contained (A) 40 mM  $\text{H}_2\text{O}_2$  in 0.1 M PBS; and (B) 1 mM hydrazine in 0.1 M PBS. Potential sweep rate,  $v = 20$  mV/s. Inset: the magnified data showing the onset of the  $\text{H}_2\text{O}_2$  oxidation current.

The oxidation of hydrazine occurs at significantly lower potentials than that of  $\text{H}_2\text{O}_2$  ( $E^\circ$  is about 0.15 V vs Ag/AgCl).<sup>20</sup> Thus, a small wave of Fc oxidation (at  $\sim 0.1$ -0.3 V; curve 1 in Figure 2B) is followed by the continuous increase in  $i$  over  $>800$  mV range. By contrast, the direct oxidation of  $\text{N}_2\text{H}_4$  at a bare CNE (curve 2 in Figure 2B) is very slow.<sup>20</sup> The sharp change in the slope of the  $i - E$  curve at higher potentials points to the onset of water oxidation. The current increase in this region at the Fc-CNE is much larger than that at the bare CNE due to the Fc mediated OER (Figure S3 shows OER voltammograms with no hydrazine present in solution). This observation suggests that the electrode potential can drive uphill the ET between a surface-bound molecular catalyst and solution species even if their redox potentials are greatly mismatched.

Density functional theory (DFT) simulations were performed to further understand the voltage-driven bimolecular ET processes. Figure 3 shows simulated plane-averaged electrostatic potentials (relative to the electrostatic potentials at the computational potential of zero charge) of a Fc-CNE electrode under various applied voltages. The electrostatic potential is equal to the electrode potential inside the slab and decays to zero in the bulk solution. A potential drop between the surface-bound mediator and the OHP, where the dissolved reactant is considered to be, appears when a positive bias is applied. The magnitude of potential drop increases with increasing bias (Figure S6). This potential drop can provide

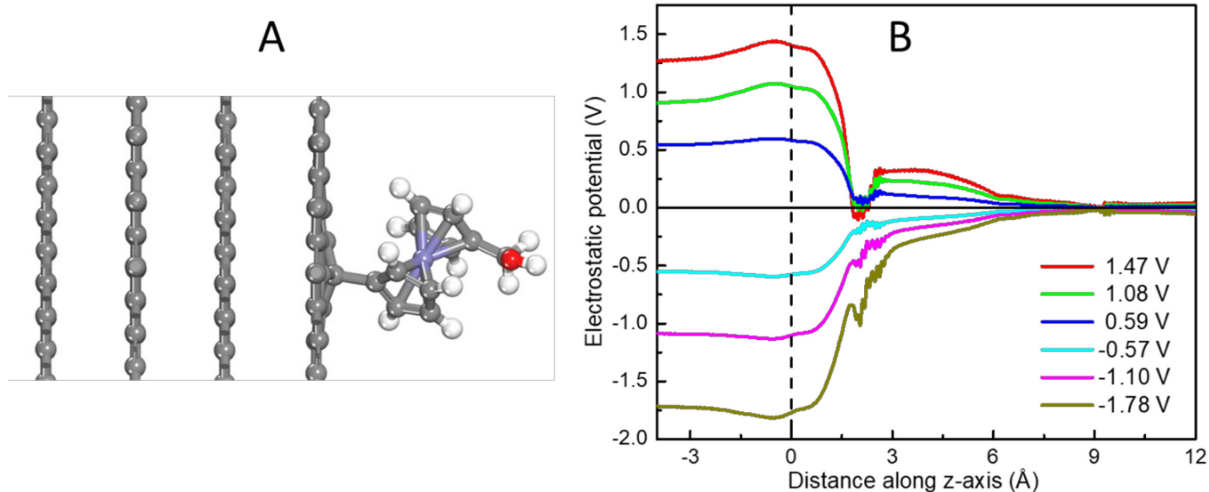


**Figure 3.** (A) The atomic structure of Fc-CNE. C, grey; H, white; O, red; Fe, purple. (B) Plane-averaged electrostatic potential of Fc-CNE at different applied voltages. The distance along z-axis of 0 Å corresponds to the electrode surface; the zero-potential region corresponds to the bulk solution.

additional driving force for the ET between the mediator and the reactant besides the chemical driving force, and explains the uphill reactions observed in our experiments. Similarly, a potential increase between the surface-bound mediator and the OHP is observed when a negative bias is applied. This suggests that, in addition to oxidation catalysis, a molecular catalyst immobilized on the electrode could also reduce substrates with more negative standard potentials. In terms of the energy levels, we find that the Fermi level of the surface-bound mediator can be shifted under the applied bias due to electronic coupling to the electrode, driving the uphill reactions (Figure S7). In a conceptually similar system—a self-assembled monolayer film anchoring a redox molecule, e.g., Fc, to the electrode surface—the potential drops almost entirely between the surface and the attached redox centers. A minor part of the potential dropping between the Fc and solution results in a shift in the apparent formal potential of Fc.<sup>21</sup>

Figure S8 shows the simulated plane-averaged electrostatic potential and ionic excess profile for a bare CNE at a positive bias. Due to the specific adsorption of ions, there is a potential decrease from the OHP to IHP. This impedes ET from the dissolved reactant to the electrode and explains the very slow catalysis observed at the bare CNE. Likewise, because of the specific adsorption, there are potential valleys/peaks near the carbon surface when positive/negative bias is applied to the Fc-CNE (Figure 3B). Thus, ET between the dissolved reactant and the underlying carbon is also unlikely to occur in the presence of a surface-bound mediator. Additionally, a shorter distance between the dissolved reactant and the mediator further facilitates ET between them, as the ET rate constant decays exponentially with the separation distance.

It is important to exclude the possibility that the observed potential-dependent electrocatalysis is an artifact caused by the formation of metal or metal oxide residues via decomposition of the metal complexes on the CNE surface. Although there is no evidence in the literature of such processes involving either Ru(bpy)<sub>3</sub> or Fc in aqueous media, the decomposition of Mn-containing complexes<sup>22</sup> and ferrocene reaction with oxygen in acetonitrile<sup>23</sup> have been reported. Two control experiments showing that voltage-driven molecular catalysis is unrelated to the formation of metallic active sites on the electrode surface are discussed in Supporting Information.

Although catalytically inert CNEs are especially suitable for studying voltage-driven molecular catalysis, this phenomenon can also be observed at metal (e.g., Pt) electrodes. In the voltammogram obtained at a Fc-modified 50 nm Pt electrode (Fc-Pt; curve 1 in Figure 4A), the onset potential of the H<sub>2</sub>O<sub>2</sub> oxidation ( $\sim$ 0.25 V vs. Ag/AgCl) is more negative than that measured at the Fc-CNE (Figure 2A), suggesting that direct electrooxidation at the Pt surface contributes to the current. However, at more positive

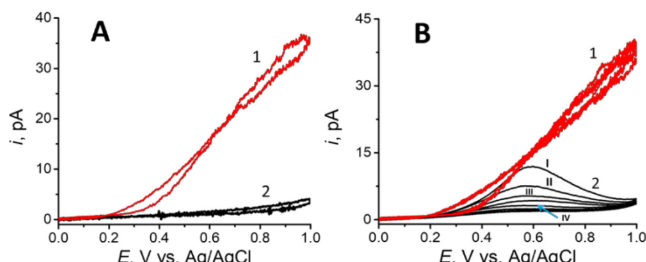


**Figure 4.** Oxidation of H<sub>2</sub>O<sub>2</sub> at Fc-Pt and bare Pt nanoelectrodes. (A) Steady-state voltammograms at the same 50 nm Fc-Pt electrode in 0.1 M PBS containing 1 mM H<sub>2</sub>O<sub>2</sub> (1) and blank PBS (2). (B) Four consecutive voltammetric cycles obtained with a Fc-Pt (curves 1) and a bare Pt (curves 2) nanoelectrodes in 1 mM H<sub>2</sub>O<sub>2</sub>.  $v = 5$  mV/s.

potentials, the H<sub>2</sub>O<sub>2</sub> oxidation current at a bare Pt nanoelectrode decreases sharply due to surface passivation and almost vanishes after four voltammetric cycles (Figure 4B, curves 2). By contrast, four consecutive voltammograms recorded at a Fc-Pt nanoelectrode (curves 1) show no signs of surface passivation, and the increase in anodic current over  $\sim$ 600 mV range points to voltage-driven molecular catalysis.

The immobilization of the redox mediator on the electrode surface without any spacer results in fast ET to (from) the electrode and a significant potential drop between the surface-bound catalyst and dissolved substrate, thus revealing the effect of electrode bias on the rate of molecular catalysis that was not previously observed at chemically modified electrodes.<sup>4</sup> The voltage applied across the interface between two immiscible electrolyte solutions can also contribute to the driving force for the catalytic ET between molecules confined to the different phases.<sup>24</sup> However, for such reactions the attainable interfacial potential drop is typically limited by the width of the polarization window.

In summary, we demonstrated that the applied voltage contributes to the driving force for ET between a molecular catalyst attached to the electrode surface and dissolved molecules. Such reactions can be driven uphill, e.g., Fc<sup>+</sup> and Ru(bpy)<sub>3</sub><sup>3+</sup> can oxidize water. Hybrid voltage-assisted molecular catalysts are noble-metal-free and do not suffer from passivation and surface fouling, which typically affect the performance of electrocatalysts.

## ASSOCIATED CONTENT

**Supporting Information.** Experimental details, protocols for chemical modification of CNEs, additional current-time recordings and voltammograms, TEM images of CNEs, control experiments, computational methods and additional computational results, including Figures S1 – S10. This material is available free of charge via the Internet at <http://pubs.acs.org>.

## AUTHOR INFORMATION

$\pm$  K.B. and X.W. contributed equally to this work.

## Corresponding Authors

\* [guoxiang.hu@qc.cuny.edu](mailto:guoxiang.hu@qc.cuny.edu), [mmirkin@qc.cuny.edu](mailto:mmirkin@qc.cuny.edu)

## Notes

The authors declare no competing financial interests.

## ACKNOWLEDGMENT

The support of this work by the National Science Foundation grant CHE-1900463 (MVM) is gratefully acknowledged.

## REFERENCES

- Li, J.; Triana, C. A.; Wan, W.; Adiyeri Saseendran, D. P.; Zhao, Y.; Balaghi, S. E.; Heidari, S.; Patzke, G. R. Molecular and heterogeneous water oxidation catalysts: recent progress and joint perspectives. *Chem. Soc. Rev.* **2021**, 50, 2444–2485.
- Boettcher, S. W.; Surendranath, Y. Heterogeneous electrocatalysis goes chemical. *Nat. Catal.* **2021**, 4, 4–5.
- Fourmond, V.; Plumeré, N.; Léger, C. Reversible catalysis. *Nat. Rev. Chem.* **2021**, 5, 348–360.
- Molecular Design of Electrode Surfaces, Techniques in Chemistry; Murray, R. W., Ed.; Wiley and Sons: New York, 1992, 448 p.
- Savéant, J.-M. Molecular Catalysis of Electrochemical Reactions. Mechanistic Aspects. *Chem. Rev.* **2008**, 108, 2348–2378.
- Fuel cell catalysis: a surface science approach, Koper, M. T. M., Eds.; Wiley, 2009, 720 p.

(7) Jaramillo, T. F.; Jørgensen, K. P.; Bonde, J.; Nielsen, J. H.; Horch, S.; Chorkendorff, I. Identification of Active Edge Sites for Electrochemical H<sub>2</sub> Evolution from MoS<sub>2</sub> Nanocatalysts. *Science*. **2007**, *317*, 100-102.

(8) Jackson, M. N.; Surendranath, Y. Molecular Control of Heterogeneous Electrocatalysis through Graphite Conjugation. *Acc. Chem. Res.* **2019**, *52*, 3432–3441.

(9) Nong, H. N.; Falling, L. J.; Bergmann, A.; Klingenhof, M.; Tran, H. P.; Spöri, C.; Mom, R.; Timoshenko, J.; Zichittella, G.; Knop-Gericke, A.; Piccinin, S.; Pérez-Ramírez, J.; Cuena, B. R.; Schlögl, R.; Strasser, P.; Teschner, D.; Jones, T. E. Key role of chemistry versus bias in electrocatalytic oxygen evolution. *Nature*. **2020**, *587*, 408–413.

(10) Li, F.; Li, Y. C.; Wang, Z.; Li, J.; Nam, D.-H.; Lum, Y.; Luo, M.; Wang, X.; Hung, S.-F.; Chen, B.; Wang, Y.; Wicks, J.; Li, Y.; Dinh, C.-T.; Wang, Y.; Zhuang, T.-T.; Sargent, E. H. Cooperative CO<sub>2</sub>-to-ethanol conversion via enriched intermediates at molecule–metal catalyst interfaces. *Nat. Catal.* **2020**, *3*, 75–82.

(11) Wu, L.; Nayak, A.; Shao, J.; Meyer, T. J. Crossing the bridge from molecular catalysis to a heterogenous electrode in electrocatalytic water oxidation. *Proc. Natl. Acad. Sci. USA*. **2019**, *116*, 11153–11158.

(12) Luo, S.-X. L.; Liu, R. Y.; Lee, S.; Swager, T. M. Electrocatalytic Isoxazoline–Nanocarbon Metal Complexes. *J. Am. Chem. Soc.* **2021**, *143*, 10441–10453.

(13) Jackson, M. N.; Kaminsky, C. J.; Oh, S.; Melville, J. F.; Surendranath, Y. Graphite Conjugation Eliminates Redox Intermediates in Molecular Electrocatalysis. *J. Am. Chem. Soc.* **2019**, *141*, 14160–14167.

(14) Peljo, P.; Scanlon, M. D.; Olaya, A. J.; Rivier, L.; Smirnov, E.; Girault, H. H. Redox Electrocatalysis of Floating Nanoparticles: Determining Electrocatalytic Properties without the Influence of Solid Supports. *J. Phys. Chem. Lett.* **2017**, *8*, 3564–3575.

(15) Bard, A. J. Inner-Sphere Heterogeneous Electrode Reactions. *Electrocatalysis and Photocatalysis: The Challenge. J. Am. Chem. Soc.* **2010**, *132*, 7559–7567.

(16) Barman, K.; Wang, X.; Rui, J.; Mirkin, M. V. Mediated Charge Transfer at Nanoelectrodes: a New Approach to Electrochemical Reactivity Mapping and Nanosensing. *J. Am. Chem. Soc.* **2021**, *143*, 23, 8547–8551.

(17) Bard, A. J.; Faulkner, L. R., *Electrochemical Methods: Fundamentals and Applications*, 2nd ed. John Wiley & Sons, New York, 2001, p. 13.

(18) Vanysek, P. Electrochemical Series. In *Handbook of Chemistry and Physics*, 93rd ed.; Haynes, William M. Eds.; CRC Press, 2012, pp 5–80.

(19) Connelly, N. G.; Geiger, W. E. Chemical Redox Agents for Organometallic Chemistry. *Chem. Rev.* **1996**, *96*, 2, 877–910.

(20) Miao, R.; Compton, R. G. The Electro-Oxidation of Hydrazine: A Self-Inhibiting Reaction. *J. Phys. Chem. Lett.* **2021**, *12*, 6, 1601–1605.

(21) White, H. S.; Smith, C. P. Theory of the Interfacial Potential Distribution and Reversible Voltammetric Response of Electrodes Coated with Electroactive Molecular Films. *Anal. Chem.* **1992**, *64*, 2398–2405.

(22) Najafpour, M. M.; Moghaddam, A. N.; Dau, H.; Zaharieva, I. Fragments of Layered Manganese Oxide Are the Real Water Oxidation Catalyst after Transformation of Molecular Precursor on Clay. *J. Am. Chem. Soc.* **2014**, *136*, 7245–7248.

(23) Zotti, G.; Schiavon, G.; Zecchin, S.; Favretto, D. Dioxygen-decomposition of ferrocenium molecules in acetonitrile: The nature of the electrode-fouling films during ferrocene electrochemistry. *J. Electroanal. Chem.* **1998**, *456*, 217–221.

(24) Gschwend, G. C.; Olaya, A.; Peljo, P.; Girault, H. H. Structure and reactivity of the polarised liquid-liquid interface: what we know and what we do not. *Curr. Opin. Electrochem.* **2020**, *19*, 137–143.

For TOC only

